

Micrometer-sized nozzles and skimmers for the production of supersonic He atom beams

J. Braun, P. K. Day, J. P. Toennies, G. Witte, and E. Neher

Citation: [Review of Scientific Instruments](#) **68**, 3001 (1997); doi: 10.1063/1.1148233

View online: <http://dx.doi.org/10.1063/1.1148233>

View Table of Contents: <http://scitation.aip.org/content/aip/journal/rsi/68/8?ver=pdfcov>

Published by the [AIP Publishing](#)

Articles you may be interested in

Note: [Manipulation of supersonic atomic beams with static magnetic fields](#)

J. Chem. Phys. **139**, 096103 (2013); 10.1063/1.4819897

[A modification of the laser detonation-type hyperthermal oxygen atom beam source for a long-term operation](#)

Rev. Sci. Instrum. **79**, 073109 (2008); 10.1063/1.2957613

[Anomalous attenuation at low temperatures in high-intensity helium beam sources](#)

Rev. Sci. Instrum. **76**, 123111 (2005); 10.1063/1.2149008

[Study of He flow properties to test He dimer potentials](#)

J. Chem. Phys. **119**, 1433 (2003); 10.1063/1.1580801

[A triply differentially pumped supersonic beam target for high-resolution collision studies](#)

Rev. Sci. Instrum. **71**, 4070 (2000); 10.1063/1.1319343



Micrometer-sized nozzles and skimmers for the production of supersonic He atom beams

J. Braun,^{a)} P. K. Day,^{b)} J. P. Toennies, and G. Witte^{c)}
Max-Planck-Institut für Strömungsforschung, D-37073 Göttingen, Germany

E. Neher
Max-Planck-Planck-Institut für Biophysikalische Chemie, D-37077 Göttingen, Germany

(Received 15 April 1997; accepted for publication 21 May 1997)

Micrometer-sized nozzles and skimmers made from drawn glass tubes are described and tested for the production of highly monoenergetic He atom beams. Glass nozzles with diameters between 1 μm and 4 μm when operated at He source stagnation pressures of up to 1000 atm provide intense beams with measured speed ratios of $S=50$ –100, in good agreement with the predicted behavior scaled from nozzles with larger openings. Miniature glass skimmers with diameters as small as 3 μm were also successfully tested with conventional 10 μm diameter nozzles. These miniature nozzle-beam sources can be used to greatly reduce the size of present-day He-atom surface-scattering time-of-flight spectrometers and to reduce the number of vacuum stages and the size of vacuum pumps. They also open up new experimental possibilities as illustrated by measurements of the spatial profiles of seeded nozzle beams. © 1997 American Institute of Physics. [S0034-6748(97)05308-2]

I. INTRODUCTION

Highly monochromatic thermal atomic beams, generated by sampling the core of a supersonic expansion of a gas through a small orifice with a sharp-edged conical skimmer, are used in numerous areas of research in physics and chemistry.¹ Important applications have been found in such diverse fields as Doppler-free laser spectroscopy,² crossed-beam reactive and inelastic scattering,³ *in situ* monitoring of crystal-growth,^{4,5} elastic and inelastic surface scattering,^{6,7} and, recently, atom and molecule optics.⁸ For most of these experiments a high monochromaticity and a high specific beam source intensity $\mathcal{I}(\mathcal{I}=d^2I/d\omega dv$, where I is the intensity in atoms/s, $d\omega$ is the solid angle at the detector and dv is a beam velocity interval) are important.⁹ For atom and molecule optics the specific brightness, given by $\mathcal{B}=\mathcal{I}/A_{\text{eff}}$, where A_{eff} is the effective area of the source, can however be of crucial significance. The actual effective source area of a nozzle beam source is larger than given by the nozzle cross section A_0 since the free particle beam is emitted from an effective sudden freeze (SF) area A_{SF} , which is downstream from the orifice and is therefore considerably larger than A_0 . In the present case where the skimmer openings are much smaller than A_{SF} , \mathcal{B} is determined by the skimmer opening A_{SK} . A high specific brightness is not only required for atom optical devices but also, as discussed below, can lead to a reduction in the size and cost of a high-resolution helium-atom surface-scattering apparatus.

Although nozzle beams have been produced from most gases,¹ helium atom beams represent an exceptional case because of their very high degree of monochromaticity.¹⁰ This

has been shown to be due to a quantum effect related to the very weak binding energy of only 1.1×10^{-7} eV of the He dimer.¹¹ This leads to an extraordinary increase in the integral cross section at low ambient gas temperatures below 1 K which effectively drives the expansion¹⁰ to even lower temperatures of about 10^{-3} K that would not otherwise be reached. Experimentally, the velocity resolution is characterized by the speed ratio, S , which is related to the mean beam velocity v and the full width at half-maximum (FWHM) of the velocity distribution Δv by $S=1.65v/\Delta v$. For helium, speed ratios as high as $S=500$ (Ref. 12) have been achieved in continuous flow and $S=1530$ (Ref. 13) in pulsed-beam operation.

For all gases at a fixed source temperature that is sufficiently high to avoid cluster formation the speed ratio is found to vary approximately with source stagnation pressure P_0 and the nozzle diameter d according to $S\propto(P_0\cdot d)^{1/2}$,¹⁰ while the total gas flux Φ varies as $\Phi\propto P_0\cdot d^2$. Thus, since $S\propto(\Phi/d)^{1/2}$, the speed ratios increase with decreasing nozzle diameter for a given total gas flux, which is limited by the pumping speed in the nozzle chamber. The specific brightness \mathcal{B} for a given speed ratio is approximately proportional to $P_0^{1/2}$. Since, moreover, A_{SF} is proportional to d for a given flux, the size of the pumps can be decreased by reducing d and increasing P_0 . Alternatively, for a given speed ratio S and specific brightness the flux can be reduced by using smaller diameter nozzles.

Finally, as a general consequence of the above, a reduction in d can in principle lead to a reduction in the overall dimensions of a scattering apparatus and under certain circumstances can also lead to an overall gain in the signal to noise ratio. The latter effect can be understood by noting that the pumping speeds of the differential pumping stages in a modern high resolution helium-atom surface scattering apparatus scale roughly with the square of the overall dimensions of the machine, whereas the signal arriving at the detector is

^{a)}Electronic mail: braun@msft14.dnet.gwdg.de

^{b)}Present address: Jet Propulsion Laboratory, 4800 Oak Grove Drive, Pasadena, CA 91109.

^{c)}Present address: National Center for Electron Microscopy, Lawrence Berkeley Laboratory, One Cyclotron Road, Berkeley, CA 94720.

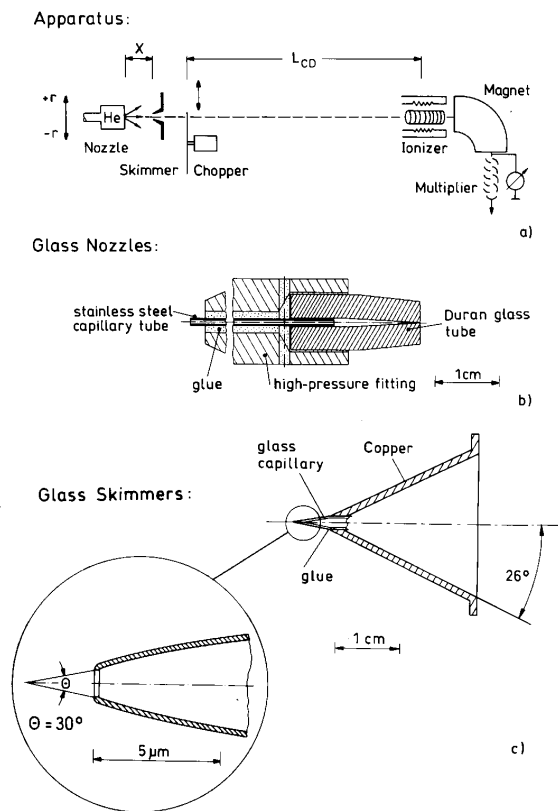


FIG. 1. (a) Schematic diagram of the helium-atom nozzle beam time-of-flight apparatus used to characterise the miniature nozzles and skimmers. (b) A scale drawing of the cross section through the high pressure miniature nozzle holder. (c) A scale drawing of the cross section of the miniature skimmer holder. The end of a miniature skimmer is shown on an expanded scale on the left side (Ref. 27). The opening angle is to 30° .

proportional to the inverse of the square of the beam path length.

In the present article the intensities and speed ratios of the He-atom free jet beams produced by capillary micron-sized glass nozzles operated at source pressures up to 1000 bar are investigated. In addition, micron-sized glass skimmers were investigated using conventional nozzles. The experimental apparatus and the fabrication of the miniature capillary nozzles and skimmers are described in Section II. The measurements are described in Section III and in Section IV. The article closes with a discussion and the outlook for possible applications. Appendix A contains an estimate of the pressure drop in the long narrow miniature nozzles used, whereas in Appendix B the results of the calculation of the mole fractions of small He clusters at high source pressures are presented.

II. EXPERIMENTAL SETUP

A. Apparatus

Figure 1(a) shows a schematic diagram of the atom beam apparatus used to characterize the beam properties. The helium-atom beam is formed by a supersonic expansion from a high source pressure of up to 1000 bar into a high-vacuum chamber. This chamber is designed to handle a large gas flux and is thus evacuated by an unbaffled 6000 ℓ/s oil diffusion pump followed by a 253 m^3/h mechanical Roots blower. With this arrangement a helium-gas throughput of up

to about 3 mbar ℓ/s can be maintained at a chamber pressure of about 5×10^{-4} mbar. After passing through a conical skimmer as described in more detail below and through three differential pumping stages (not shown in Fig. 1) the helium atoms are detected in an ultrahigh vacuum (UHV) chamber (base pressure 1×10^{-10} mbar) by a home-made electron bombardment ioniser followed by a 90° magnetic mass spectrometer. For time-of-flight (TOF) analysis the beam is mechanically chopped (pulse width 5–20 μs) by a high speed (300 Hz) rotating slotted disc and the ion signal is detected after a total flight path of $L_{CD} = 0.82$ m. The ionisation length of 4 mm limits the velocity resolution to about $\Delta v/v = 1.5\%$ ($S \cong 110$).¹⁴ Apertures between the differential pumping stages and the ionisation region of the detector define the beam divergence to about 0.2° which corresponds to a detected solid angle of about 1.3×10^{-5} steradian. The distance between skimmer and detector amounts to $L_{SKD} = 1.12$ m. The high source pressures were achieved using an air driven compressor.¹⁵

The conventional sources used routinely in our laboratory consist of a commercially available electron microscope aperture lens,¹⁶ with a hole diameter of typically 10 μm and an orifice length of about 30 μm , followed by a home-made conical nickel skimmer. In the present experiments a skimmer that had an unusually large 1.6 mm inside diameter (i.d.) opening was used, whereas skimmers with about 0.6 mm i.d. are typically used.¹⁷ This, however, should have no appreciable effect on the intensities and speed ratios in the present measurements. The other dimensions such as the internal angle of 25° and external angle of 32° and an overall length of about 27 mm and lip edges with a width of better than 5–10 μm were the same as the conventional skimmers. The experiments described here were carried out by replacing either the nozzle or the skimmer with the corresponding glass parts. The distance x between nozzle and skimmer and also the offset $\pm r$ perpendicular to the beam axis (see Fig. 1) could be varied by moving the nozzle with the help of set screws with an accuracy of $\pm 2 \mu m$. All the measurements presented here were performed at room temperature at which the He-atom beam has a kinetic energy of about 80 meV.

B. Miniature nozzles

The construction and mounting of the miniature glass nozzles are shown in Fig. 1(b). Similar glass nozzles have been used frequently in the past, but apparently with openings typically 20 μm or larger.¹⁸ The present nozzles were drawn from thick-walled [4 mm outside diameter (o.d.) 0.6 mm i.d.]. Duran Glass high-pressure capillaries, in this case until the inner channel closed completely.¹⁹ The tubes were then cut in the middle of the drawn sections and the new ends ground back until openings of the desired diameter of about 1 μm appeared. A trivial but severe problem was clogging of the nozzle orifice by particles as a consequence of the grinding process. In order to clear the nozzle, the capillary was first sonicated for 20 min in a detergent, and then carefully rinsed with filtered, distilled water both on the outside and the inside. For the latter a polyethylene tube, drawn out to a tip of approximately 20 μm and connected to a syringe, was used. Subsequently, fluid was removed from the inside

using the same tube. The inner wall of the capillary was then dried by a stream of dry nitrogen, again delivered through a thin polyethylene tube. During all these manipulations the nozzle tip was immersed in filtered, distilled water. At this stage it could be ascertained if the nozzle were clear, since the water would then slowly enter by capillary action. In this case this water was again removed while the nozzle tip was transferred to methanol. Again, fluid (methanol) was allowed to enter the capillary and be continuously removed. As a final step, pressure was applied to expel methanol from the nozzle. The pressure required to expel and to form air bubbles in the methanol is a convenient measure of the nozzle diameter.¹⁹ Pressure is maintained while the nozzle is removed from the methanol until the surface is completely dry.

In the apparatus He gas was supplied through a miniature stainless steel capillary tubing (0.5 mm o.d., 0.25 mm i.d.).²⁰ One end of the tubing was inserted into the open end of the glass nozzle. The capillary and nozzle were then glued²¹ into a high-pressure fitting,²² taking care that the glue completely filled the region between the i.d. of the glass tube and that of the high-pressure fitting and the o.d. of the capillary [see Fig. 1(b)]. This construction has the advantage that the high pressure is applied only to the small surface area of the inner wall of the stainless steel capillary tube and the Duran glass tube so that the overall forces on these components are kept small.

Compared to the commonly used nozzles made from electron-microscope apertures, these nozzles have long tapered channels. The effect of the pressure drop over the length of the channel is estimated in Appendix A and is found not to be significant. The nozzle pressures for all data reported in this article were measured at the gas inlet line. Stoppage in the miniature nozzles could be largely avoided by carefully cleaning the gas supply tubing by rinsing the tubes in acetone before attaching them to the nozzle block described above, and by passing the gas through a liquid-nitrogen trap and a 0.5 μm filter²³ in the supply line directly in front of the nozzle.

C. Miniature skimmers

The miniature skimmers are micropipettes produced according to the techniques developed for patch-clamp probing of single nerve cells.^{24–27} The micropipettes are drawn from a thin walled Pyrex glass²⁸ tube (2 mm o.d. and 1.6 mm i.d.). The micropipette fabrication process has been extensively investigated^{25,26} and micropipette pullers especially developed for this purpose and available commercially²⁹ were also used here to provide a controlled axial force. As the hot tube contracts during pulling, the ratio of the o.d. and the i.d. remains nearly constant. Figure 1(c) shows the construction of the miniature skimmers and a diagram of the cross section of the end of a typical pipette.²⁷ The diameter of the orifice obtained after breaking the tube in the middle can be varied over a range of 1–25 μm (Ref. 30) through the heating parameters and the force applied. Figure 2 shows electron-microscope photographs of one of the 2 μm glass skimmer used in the present experiments. The opening is almost perfectly circular. The opening lip for a 2 μm diameter orifice is

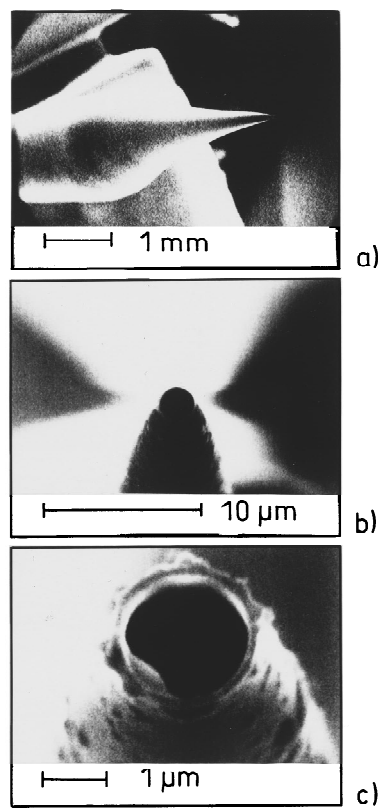


FIG. 2. Electron-microscope photos taken of a 1.5 μm skimmer. Note the almost perfect form of the opening and the sharpness of the end of the skimmer. The magnification is (a) 20 \times , (b) 4600 \times , and (c) 20000 \times .

estimated from the photographs to have a thickness of 0.2 μm . The opening angle Θ [see Fig. 1(c)] was measured using the light microscope at about 30 $^\circ$, whereas the skimmers with diameters larger than 10 μm had opening angles of about 12 $^\circ$. Since accurate measurement of the opening diameter with an electron microscope (as shown in Fig. 2) required destruction of the parts, the diameters of most of the miniature nozzles and skimmers were measured with an optical microscope that was calibrated by comparison with the electron-microscope picture. Because these measurements suffered greatly from resolution and contrast problems, the values quoted are only approximate and have an estimated uncertainty of about 0.5 μm .

III. MINIATURE NOZZLE MEASUREMENTS

The terminal speed ratios versus $P_0 d$ measured for helium using three different capillary type nozzles with orifice diameters d of 1, 4, and 10 μm are presented in Fig. 3(a). The measurements with the miniature nozzles were made with the conventional nickel skimmer described in Section II and with an intensity optimized nozzle-to-skimmer distance of about 12.5 mm. The error bars are due to uncertainty in the determination of the nozzle diameters mentioned above, which we have estimated to be $\pm 0.5 \mu\text{m}$ and $\pm 1 \mu\text{m}$ for the 1 and 4 μm nozzles, respectively. These systematic errors imply a shift of the entire curve parallel to the abscissa in either direction in Fig. 3(a) as indicated by the error bars. For comparison, the dashed curve shows the results of earlier measurements with a 10 μm nozzle and a factor of 2 larger

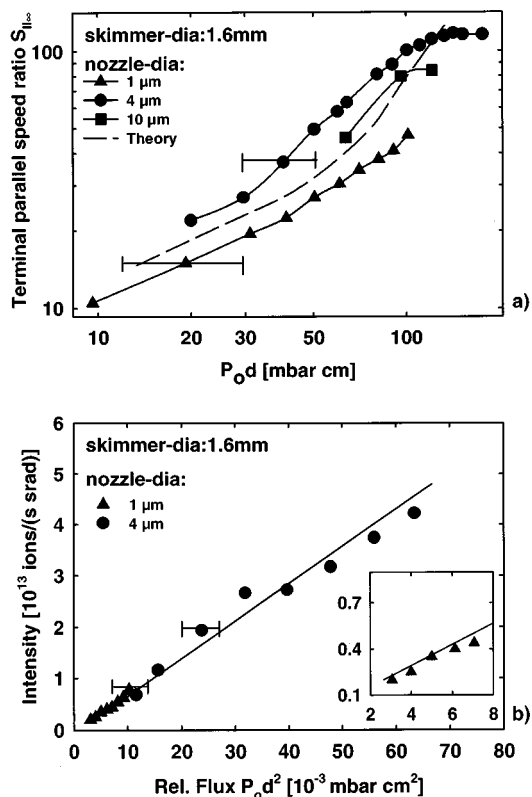


FIG. 3. (a) Speed ratios for various nozzle pressures for a 1 μm nozzle (triangles) and a 4 μm nozzle (circles). The error bars represent the uncertainty in the nozzle-diameter measurement. For comparison, data for a standard 10 μm nozzle (squares) are shown. The dashed curve shows the behaviour of a helium-beam source in the limit of very large pumping speed (from Ref. 10). The nozzle-skimmer distance was 12.5 mm. (b) Helium flux, measured from the ion current on the first dynode of the detector multiplier, for the 1 and 4 μm nozzles (circles and triangles). The 1 μm skimmer data are shown in the inset, again rescaled. The nozzle-skimmer distance was again 12.5 mm.

pumping speed.¹⁰ It is seen that the new measurements with the miniature nozzles compare favorably within 12%–25% with the previously reported speed ratios.¹² These in turn are in agreement with theory [not shown in Fig. 3(a)] also to within about 10%–25%.¹⁰ Thus the present results agree within the large errors resulting from the uncertainties in d with the earlier work. This agreement provides confirmation that there is no significant pressure drop in the capillary micronozzles as was predicted theoretically (see Appendix A).

Within this general agreement several differences to the earlier results may be of significance. First of all the speed ratios for the 4 μm nozzles are larger by about 10%–20% than those measured earlier. The cause for this increase is not understood and requires further study. On the other hand, the speed ratios measured for the 1 μm nozzles are significantly smaller. The saturation to a constant value of about $S \approx 110$ at $P_0 d \geq 105$ mbar cm is in accordance with the maximum measurable speed ratio due to the limited resolution of the apparatus as described in Section II. The measurements for the 1 μm nozzle were limited to a $P_0 d$ value of 100 mbar cm by the maximum pressure available (1000 bar, see above). As discussed in Appendix B the mole fraction of dimers in the source at $P_0 = 1000$ bar and $T_0 = 300$ K is es-

timated to be less than 6×10^{-3} and should have no influence on the results.

To rule out that these effects were due to skimmer interference effects, the Knudsen number Kn at the skimmer entrance was estimated. For the conventional 25°/32° skimmer used in these experiments it has been shown theoretically³¹ that skimmer interference can be neglected if the Knudsen number Kn is greater than 2,

$$Kn (= \lambda_S / d_S) \geq 2, \quad (1)$$

where d_S is the diameter of the skimmer entrance ($d_S = 1.6$ mm) and λ_S is the mean free path of the He atoms in the beam at the skimmer location,¹

$$\lambda_S = n_S^{-1} \left[5.3 \left(\frac{C_6}{k_B T_0} \right)^{1/3} \right]^{-1}, \quad (2)$$

where the term $5.3(C_6/k_B T_0)^{1/3}$ is proportional to the classical integral collision cross section of two He atoms [$C_6/k_B = 10^{-43}$ K cm⁶, $T_0 = 300$ K (Ref. 1)] and n_S is the number density at the skimmer location. The latter can be predicted from the terminal Mach number M

$$n_S = \frac{P_0}{RT_0} \left(1 + \frac{\gamma-1}{2} M^2 \right)^{-1/\gamma-1}, \quad (3)$$

where [1]

$$M = B \left(\frac{x}{d} \right)^{\gamma-1} - \frac{\gamma-1}{\gamma+1} \frac{1}{2B \left(\frac{x}{d} \right)^{\gamma-1}}. \quad (4)$$

In Eq. (4) d and x are the nozzle diameter and the nozzle-to-skimmer distance, respectively, and the constant B is given by $B = 3.26$.¹ For the maximum values of $P_0 d$ used in the present experiments of 100 mbar cm ($d = 1$ μm), 300 mbar cm ($d = 4$ μm) and 130 mbar cm ($d = 10$ μm) the Knudsen numbers predicted using Eqs. (1)–(4) are 130, 11, and 8, respectively. Since they are well above the limit of $Kn = 2$, given in Eq. (2), any significant deterioration of the beam due to skimmer interference seems unlikely.

A reduction of the speed ratio for large values of $P_0 d$ due to scattering from the residual gas in the region between the nozzle and skimmer can also be neglected. The smallest value of mean-free-path length λ_S [see Eq. (2)] for scattering by the residual gas in this region occurs for $d = 10$ μm and the highest source pressures, in which case $\lambda_S \approx 13$ mm. It must be realized that single collisions with the residual gas scatter the beam particles out of the forward direction of the beam and thus lead only to a attenuation. In order to degrade the speed ratio, the scattered particles must undergo at least one or two additional collisions in order to be scattered back into the forward beam direction.

Figure 3(b) shows the total intensity per solid angle expressed in terms of the detected ion current versus $P_0 d^2$ for the 1 and 4 μm nozzles. The ion current was measured with a commercial electrometer amplifier at the first dynode of the electron multiplier with the multiplier voltage turned off (see Fig. 1). The electron impact ioniser has an ionisation probability for He atoms of approximately 5×10^{-6} with a rather

large uncertainty of about $\pm 1.5 \times 10^{-6}$. Thus to obtain the absolute intensity in atoms/s the ordinate values have to be multiplied by a factor of about 2×10^5 . For both miniature nozzles the expected linear increase of the beam intensity proportional to the total flux $P_0 \cdot d^2$ is observed. The intensity measured with a conventional $10 \mu\text{m}$ nozzle held at room temperature ($P_0 = 200$ bar, nozzle-to-skimmer distance 18 mm) is a factor of 3 greater than that for the $4 \mu\text{m}$ nozzle under the conditions given above. This agrees within a factor of about 2 with the ratio of the areas of these nozzles $A_{10}/A_4 = 10^2/4^2 \approx 6$.

In summary, it is gratifying to see that the observed terminal speed ratios follow within the large errors in d roughly the predicted behavior of conventional helium-atom nozzle beam sources that is indicated by the dashed curve in Fig. 3(a).¹⁰ Thus we conclude that the miniature capillary micronozzles tested in the present experiments are able to produce atom beams with the same high terminal speed ratios as those obtained with the conventional short nozzles at equivalent values of $P_0 d$.

IV. MINIATURE SKIMMER MEASUREMENTS

The miniature skimmer experiments were carried out using a conventional $10 \mu\text{m}$ electron-microscope-aperture sharp-edged metal nozzle (see Section II) at room temperature and a stagnation pressure of 120 bar corresponding to $P_0 d = 120$ mbar cm. Since in initial experiments the skimmers with diameters of less than $5 \mu\text{m}$ quickly became clogged with oil, the un baffled source-chamber diffusion pump used in the experiments described in the Section III was replaced with a 1500 ℓ/s turbo pump. The estimated total gas flow that could be handled with this pumping system was estimated to be 0.15 mbar ℓ/s at a typical operating pressure of 1×10^{-4} mbar. After careful alignment of the skimmer at each point, the intensity and the speed ratio versus the nozzle-to-skimmer distance were recorded. The data are shown in Figs. 4(a) and 4(b).

The speed ratios, recorded for 3, 5, and $10 \mu\text{m}$ skimmers [Fig. 4(a)], increase slightly with increasing nozzle-to-skimmer distance. The maximum value of $S = 78$ measured for the $10 \mu\text{m}$ diameter skimmer is in agreement with measurements in a separate experiment with a 1.6 mm diameter skimmer under the same stagnation conditions [not shown in Fig. 4(a)]. Lower maximum speed ratios of 65 and 24 were found for $5 \mu\text{m}$ and $3 \mu\text{m}$ diameter skimmers, respectively. Experiments were also attempted with a $1.5 \mu\text{m}$ diameter skimmer but no satisfactory beam could be produced. This could be due to our inability to properly align the small diameter skimmers that tended to be somewhat crooked [see Fig. 2(a)]. Thus it cannot be ruled out that a part of the incident beam collided with the skimmer walls and lead to a complete attenuation of the beam.

In Fig. 4(a) the variation of speed ratio with nozzle-skimmer distance is compared with curves for $P_0 d = 80$ and 800 mbar cm reported in Ref. 10. It is seen that the values $P_0 d = 120$ mbar cm used in the experiments for the two larger skimmers are located as expected between the lines corresponding to 80 mbar cm and 800 mbar cm and show approximately the predicted increase with the nozzle-

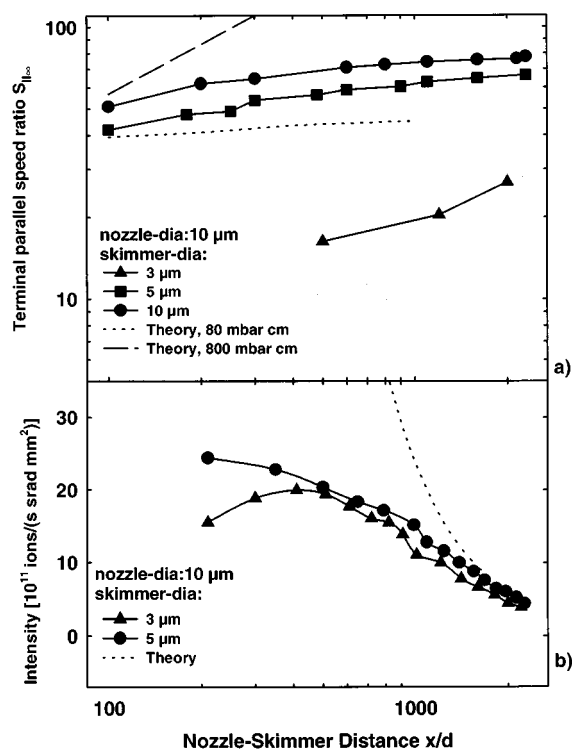


FIG. 4. (a) Speed ratios vs nozzle-to-skimmer distance for $10 \mu\text{m}$ (circles), $5 \mu\text{m}$ (squares), and $3 \mu\text{m}$ (triangles). All measurements use a standard nozzle ($d = 10 \mu\text{m}$, $P_0 = 120$ bar, $P_0 d = 120$ mbar cm). The dotted and the dashed lines represent the theoretical values predicted in Ref. 10 for 80 mbar cm and 800 mbar cm, respectively. (b) Helium flux, estimated from the ion current measured on the first dynode of the detector multiplier [see Fig. 1(a)], vs nozzle-to-skimmer distance for miniature skimmers with $3 \mu\text{m}$ (triangles) and $5 \mu\text{m}$ (squares) diameters. The dotted line shows the predicted $(x/d)^{-2}$ behaviour.

skimmer distance. Hence, for these two skimmers, the observed variations appear to reflect the expected behavior. However, the values measured for the $3 \mu\text{m}$ diameter skimmer are dramatically smaller than predicted. The much reduced speed ratios would seem to indicate significant skimmer interference which, since d_s is now smaller than in the micronozzle experiments, cannot be explained by the criterion in Eq. (1). More likely this discrepancy may reflect (a) geometrical imperfections of the skimmer and/or (b) imperfections of the sharp lip edges and/or (c) difficulties of aligning the skimmer axis with the free-jet axis to avoid collisions of beam molecules with the skimmer interior.

Figure 4(b) shows the nozzle-skimmer-distance dependence of the measured He-atom flux estimated from the detector count rate divided by the area of the skimmer opening πd_s^2 for the two smallest skimmers. Since the sudden freeze area A_{SF} is definitely much larger than the area of the microskimmer openings, the beam fluxes should be the same unless there is significant choking resulting from skimmer interference. The good agreement with the dashed line which shows the expected x^{-2} dependence indicates that there is no choking for $x/d > 1200$. The increasing deviations from the ideal behavior at $x/d < 1200$ is a strong indication of skimmer interference since the sudden freeze surface of the system is located at smaller distances of $x/d \approx 200$. These deviations correlated with the slight dropoff in speed ratios

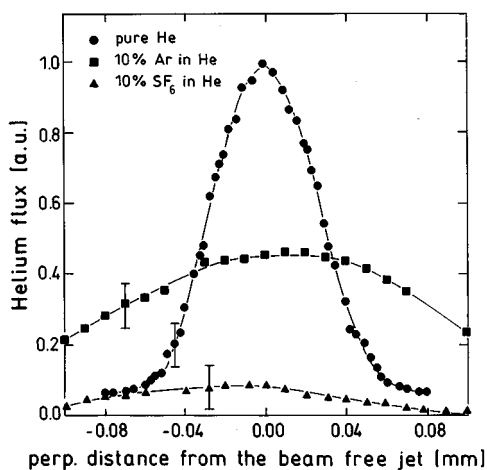


FIG. 5. Beam profiles for pure helium and two different mixtures recorded by moving the miniature skimmer (diameter: $10\ \mu\text{m}$) perpendicular to the beam axis. The source parameters were $P_0=120\ \text{bar}$, $d=10\ \mu\text{m}$ ($P_0d=120\ \text{mbar cm}$) and a nozzle-skimmer distance of $2\ \text{mm}$.

also observed at $x/d < 1200$ in Fig. 4(a). At the present time more measurements are needed to understand the origin of this strong skimmer interference. Again small misalignments of the narrow skimmers will easily lead to internal skimmer stoppage. Additional experiments with specially designed skimmers with larger opening angles are being prepared.³²

As an example application of these new miniature skimmers, we have measured intensity profiles of seeded beams from nozzle sources using a $10\ \mu\text{m}$ glass skimmer. Seeded nozzle beams have been long used in atomic and molecular-beam experiments as a method of either changing the velocity of a particular species or as a method of improving the velocity distribution of a particular species by seeding in helium.^{1,33,34} A seeded species will be accelerated or decelerated if it is heavier or lighter than the carrier gas, respectively. The limiting factor is that the lighter species diffuses laterally out of the beam so that the intensity greatly decreases with increasing mass mismatch. Also, skimmers are frequently used in molecular-beam-mass spectrometer sampling systems and the composition distortion in mixtures resulting from different rates of lateral diffusion must be accounted for in interpreting the measurements.³⁴ The present experiments were carried out by moving the $10\ \mu\text{m}$ diameter nozzle perpendicular to the beam axis and the skimmer axis, indicated by a double-headed arrow denoted by $\pm r$ in Fig. 1(a). Figure 5 compares helium intensity profiles for beams formed from seeded free jets of 10% argon in helium and 10% SF_6 in helium with a pure room temperature helium free jet. The source parameters were $P_0=120\ \text{bar}$ and a nozzle-skimmer distance of $2\ \text{mm}$ ($x/d=200$). The mass spectrometer is set in all cases at the mass of helium. The helium components of the seeded free-jet profiles are found to be much broader than those for the pure helium free jet, with that for the 10% SF_6 beam being particularly broad. The observed profile can be explained by consideration of the geometry of the apparatus and the speed ratio S of the He beam. If $S = 50$ the half-width of the beam at the detector is about $25\ \text{mm}$, so that the half-maximum intensity is expected if the source is moved by $0.04\ \text{mm}$ perpendicular to the

centerline. This is slightly larger than the measured value of $0.03\ \text{mm}$ in the beam profile of pure He in Fig. 5. The obvious nonsymmetry in the 10% SF_6 profile is not completely understood. We can attribute observation of this partially to uncertainties in the measurements in the count rate as can be seen by the error bars in Fig. 5.

V. DISCUSSION

Capillary glass micronozzles have been shown to be very useful for the production of helium-atom beams with large speed ratios similar to what is achieved using the conventional electron-microscope apertures. The advantages of micronozzles are that they can be produced with variable diameters as low as $1\ \mu\text{m}$ and that they can withstand very high pressures of at least $1000\ \text{bar}$. By going to high pressures it is possible to largely compensate for the loss of flux resulting from the smaller opening. The present experiments as confirmed by the calculations indicate that there is only a negligibly small pressure drop in the relatively long ($\approx 50\ \text{mm}$) channels of the micronozzles. One problem with going to high source pressures is the formation of clusters in the source during expansion. The equilibrium mole fractions of small He clusters was estimated for $P_0=1000\ \text{bar}$ and $P_0=500\ \text{bar}$ for various source temperatures and the results are summarized in Appendix B. From these calculations we estimate that dimers should constitute less than 5% of the gas in the source for $T_0 \geq 100\ \text{K}$, with larger clusters having at least an order of magnitude smaller concentration. A small concentration of dimers is not expected to affect the attainment of high speed ratios. More serious would be the formation of dimers and trimers and the resulting heat release during expansion. There is now some experimental evidence that appreciable clustering in the course of expansion only sets in at source temperatures below about $170\ \text{K}$ (Ref. 35) and possibly considerably lower (about $100\ \text{K}$). Thus in order to achieve high speed ratios micronozzles are limited to somewhat higher temperatures of $100\text{--}170\ \text{K}$ than conventional nozzles operated at pressures of $100\ \text{bar}$ where the lowest temperatures are about $30\text{--}40\ \text{K}$.

In addition to the glass capillary micronozzles, miniature glass skimmers were also tested in conjunction with the standard thin wall $10\ \mu\text{m}$ diameter nozzles. High speed ratios and the expected beam fluxes were obtained with skimmers with diameters as small as $5\ \mu\text{m}$. These are roughly a factor of 50 smaller than the smallest available metal skimmers.¹⁷ They have several advantages over the metal skimmers. For one, they are much cheaper to produce in a standard puller apparatus²⁹ and they may be less prone to corrosion in certain applications. In one application discussed in the present article they were used to probe the density profiles in expansions of gas mixtures.

Perhaps the most important application will be in the development of a new generation of efficient simple-to-build high resolution helium-atom surface scattering apparatuses.⁷ Because of the much smaller diameters, the gas flow from the source chamber through the skimmer is reduced by three to four orders of magnitude. In this way the many pumping stages in a modern apparatus are no longer needed. This would additionally allow for much smaller source-target distances in the apparatus. For example, a source with a mi-

crosskimmer could be used in an inexpensive apparatus for monitoring crystal growth *in situ*.⁵ When combined with a glass microcapillary nozzle operating at high pressures of several thousand bars, the same beam intensities as in current helium-atom surface scattering apparatuses should then be achievable at a greatly reduced cost.

Atom optics⁸ represents another new field of application of miniature skimmers. Experiments involving diffraction from gratings for interferometry³⁶ or for cluster-size determination,³⁷ or involving the focusing of an atomic beam with a Fresnel-zone plate³⁸ for eventual use in helium-atom microscopy,³⁹ would benefit from the high specific brightness available with a nearly ideal point beam source.

Miniature skimmers may also find application in detectors. For example, the combination of a miniature skimmer with a field-ionisation-tip neutral-atom detector^{40,41} and possibly further focussing elements (e.g., Fresnel-zone plates) could, by providing a detector with a very high degree of angular discrimination, allow for high-resolution (<1 μm) neutral-atom microscopy. In another possible direction, a miniature skimmer combined with a mass spectrometer would allow for spatially resolved mass spectrometry, for example, in the study of reaction processes.

ACKNOWLEDGEMENTS

The authors wish to thank Dr. M. Lewerenz for the calculation of cluster mole fractions presented in Appendix B and Dr. H. Legge (Deutsche Luft- und Raumfahrtanstalt, Göttingen) for helpful discussions about the pressure gradient along the nozzle tubes. They are grateful to M. Faubel for critical constructive criticism of the manuscript and to Professor E. Knuth (UCLA) for a discussion on skimmer interference. They thank Dr. P. J. Wilbrandt (Institut für Metallphysik, University Göttingen) for making the REM photos, Professor R. B. Doak (Arizona State University) for valuable help in the initial stages of the experiment and, last but not least, thank H. Wuttke and W. Sauermann for their essential technical assistance.

APPENDIX A: ESTIMATION OF THE PRESSURE GRADIENT ALONG THE BORE OF THE CAPILLARY NOZZLES

For the capillary-type nozzles used here the expected drop in pressure between the source inlet and the orifice opening is estimated. In general the prediction of the pressure drop along the nozzle channel is rather difficult because the exact shape of the inner wall of the nozzle, the friction coefficient along the wall, and the variation of the Mach number M have to be known. Moreover, a simple prediction based on the Hagen-Poiseuille formula for laminar flow is not applicable because of the high Reynolds numbers. For example, the Reynolds number Re of a 1 μm nozzle at $P_0=1000$ bar amounts to $Re=11\,000$ which is greater than the upper limit for laminar flow ($Re=2300$). An idealized and suitable approximation for the flow inside the nozzle is based on a one-dimensional, adiabatic Fanno flow⁴² of an ideal gas. The variation of the square of the Mach number M is then given by

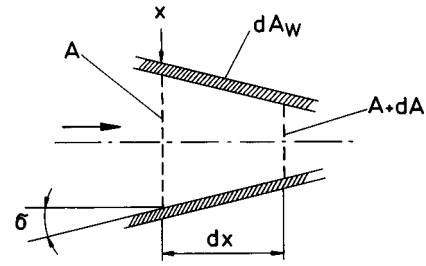


FIG. 6. Control volume and notations used for the calculation of the pressure drop along the miniature nozzle channels in Appendix A.

$$\frac{dM^2}{M^2} = -\frac{2\left(1 + \frac{\gamma-1}{2}M^2\right)}{1-M^2} \frac{dA(x)}{A(x)} + \frac{\gamma M^2\left(1 + \frac{\gamma-1}{2}M^2\right)}{1-M^2} 4f \frac{dx}{D}, \quad (\text{A1})$$

where γ is the ratio of the specific heats ($\gamma=1.67$ for He), f is the friction coefficient between the wall and the He gas, dx is the extension of the infinitesimal control volume along the inner wall of the nozzle and $A(x)$ is the area in the nozzle at position x ; (see Fig. 6). The hydraulic parameter D is defined by the following expression:

$$D = \frac{4A}{dA_w/dx}, \quad (\text{A2})$$

where dA_w is the area of the inner nozzle walls in the segment dx . Note that f is not constant along the centerline of the nozzle. Because of the lack of knowledge of an exact number for f , a wide range of values between 0.01 to 0.5 were used⁴² in the present calculations. Fortunately the predicted decrease of the pressure depends only slightly on the choice of f .

In the case of a conical duct section the ratio dx/D can be written as

$$\frac{dx}{D} = \alpha \frac{dA}{A}, \quad (\text{A3})$$

where $\alpha=1/(2\pi \tan \sigma)$ and σ is the half-angle of convergence of the capillary (see Fig. 6). For the present nozzles σ amounts to about 0.013 rad and $\alpha=12.2$. An equation similar to Eq. (A1) is obtained⁴² for the variation of the pressure along the centerline of the nozzle:

$$\frac{dP}{P} = \frac{M^2}{1-M^2} \frac{dA}{A} - \frac{\gamma M^2(1+(\gamma-1)M^2)}{2(1-M^2)} 4f \frac{dx}{D}. \quad (\text{A4})$$

If f is assumed to be constant (see above), an expression for the pressure drop is obtained by combining Eqs. (A1), (A3), and (A4):

$$\int_{P_0}^{P_{\text{orif}}} \frac{dP}{P} = \int_{M_0^2}^{M_{\text{orif}}^2} dM^2 \frac{1-2f\alpha(1+(\gamma-1)M^2)}{\left(1 + \frac{\gamma-1}{2}M^2\right)(4f\alpha\gamma M^2-2)}, \quad (\text{A5})$$

TABLE I. He cluster energy levels and degeneracies used in the calculations of Table II. The numbers in parentheses are powers of ten. N is the number of He atoms in the cluster.

N	Bonding energy (cm^{-1})	Degeneracy
1
2	0.58 (-3) ^a	1
3	0.600 (-1) ^b	1
	0.110 (-3) ^b	1
4	0.383 ^c	1
	0.700 (-1) ^c	1
5	0.942 ^c	1
	0.600 ^c	1
6	1.63 ^c	1
	1.200 ^c	3

^aReference 47.

^bReference 45.

^cReference 44.

where P_0 and M_0 are, respectively, the pressure and the Mach number at the inlet of the capillary. As shown in Ref. 43, at the orifice $M_{\text{orif}} \approx 1$. This is a good approximation if the curvature of the sonic surface is neglected.⁴³ For assumed values of $f=0.1$ the numerical integration of Eq. (A5) for nozzles with diameters ranging from 1 μm to 10 μm yields pressure drops from 2 bar to 25 bar if the initial pressure P_0 varies from 100 bar to 1000 bar, respectively. As mentioned above, similar results within 10% are obtained for $f=0.01$ and $f=0.5$ which are typical extreme values.⁴²

To summarize, for the nozzle geometries used in the experiments reported here the effects of the pressure drop along the nozzle channels is expected to be only about 2% of P_0 . This small effect is neglected and it is assumed that the pressure at the orifice is equal to P_0 rather than to the pressure P_{orif} predicted using Eq. (A5).

APPENDIX B: CALCULATION OF THE MOLE FRACTIONS OF SMALL He CLUSTERS

The mole fractions n_N of small He clusters with N atoms were calculated using standard thermodynamical statistical

TABLE II. Calculated equilibrium mole fractions of He for different values of source pressures P_0 and source temperatures T_0 . The numbers in parentheses are powers of ten. n_1 , n_2 , and n_3 denote the mole fraction of He atoms, dimers, and trimers, respectively.

Temperature (K)	n_1	n_2	n_3
$P_0=1000$ bar			
$T_0=300$	0.994	0.600 (-2)	0.47 (-4)
$T_0=200$	0.986	0.139 (-1)	0.25 (-3)
$T_0=100$	0.947	0.493 (-1)	0.33 (-2)
$T_0=50$	0.848	0.125	0.24 (-1)
$P_0=500$ bar			
$T_0=300$	0.996	0.353 (-2)	0.16 (-4)
$T_0=200$	0.981	0.869 (-2)	0.99 (-4)
$T_0=100$	0.963	0.356 (-1)	0.17 (-2)
$T_0=50$	0.875	0.107	0.17 (-1)
$T_0=20$	0.652	0.224	0.10

mechanical methods.⁴⁴ Since the bound states of the helium dimer and trimer were already calculated,⁴⁵ they can be regarded as fairly well established; those of the larger clusters were estimated and the results are summarized in Table I. The calculations also took complete account of real gas effects⁴⁶ for source pressures of $P_0 \leq 500$ bar. The calculations at 500 bar $\leq P_0 \leq 1000$ bar were obtained by an extrapolation of the equation of states to these higher pressures. These calculations have also been carried out for the P, T states along isentropic lines starting from the source conditions in order to estimate changes in the mole fractions occurring in the expansions. As found previously, the mole fractions do not change appreciably and, in view of the other uncertainties, are not given here. The source mole fractions for a wide range of high pressures and temperatures $T_0 \leq 300$ K are listed in Table II.

¹D. R. Miller, in *Atomic and Molecular Beam Methods*, edited by G. Scoles (Oxford University Press, Oxford, 1988), Vol. 1, p. 14.

²U. Hefter and K. Bergmann, in Ref. 1, Vol. 1, p. 193.

³H. Buchenau, J. P. Toennies, J. Arnold, and J. Wolfrum, *Ber. Bunsenges. Phys. Chem.* **94**, 1231 (1990).

⁴J. J. de Miguel, A. Cebollada, J. M. Gallego, J. Ferron, and S. Ferrer, *J. Cryst. Growth* **88**, 442 (1988).

⁵R. Kunkel, B. Poelsema, L. K. Verheij, and G. Comsa, *Phys. Rev. Lett.* **65**, 733 (1990).

⁶K. H. Rieder, in *Helium Atom Scattering from Surfaces*, edited by E. Hulpke (Springer, Berlin, 1992), p. 41.

⁷J. P. Toennies, in *Surface Phonons*, edited by W. Kress and F. W. de Wette (Springer, Berlin, 1991), p. 111.

⁸C. Adams, M. Sigel, and J. Mleynek, *Phys. Rep.* **240**, 143 (1994).

⁹H. Pauly and J. P. Toennies, in *Methods of Experimental Physics, Vol. 7: Atomic and Electron Physics, Atomic Interaction Part A*, edited by L. Marton (Academic, New York, 1968), p. 227.

¹⁰J. P. Toennies and K. Winkelmann, *J. Chem. Phys.* **66**, 3965 (1977).

¹¹For a recent review of He-He potentials, see, for example, A. R. Janzen and R. A. Aziz, *J. Chem. Phys.* **103**, 9626 (1995).

¹²G. Brusdeylins, H. D. Meyer, J. P. Toennies, and K. Winkelmann, *Prog. Astronaut. Aeronaut. Part II* **51**, 1047 (1977).

¹³J. Wang, V. A. Shamamian, B. R. Thomas, J. M. Wilkinson, J. Riley, C. F. Giese, and W. R. Gentry, *Phys. Rev. Lett.* **60**, 696 (1988).

¹⁴D. M. Smilgies and J. P. Toennies, *Rev. Sci. Instrum.* **59**, 185 (1988).

¹⁵We used a Nova Swiss diaphragm-type compressor (air driven), provided by the Nova Werke AG, Vogelsangstrasse 24, CH-8307 Effretikon, Switzerland.

¹⁶The electron microscope aperture lenses were provided by Plano W. Planet GmbH, PF 1329, D-35529 Wetzlar, Germany.

¹⁷Conventional skimmers were provided by Beam Dynamics Inc., 708 East 56th St., Minneapolis, MN 55417.

¹⁸J. P. Moran, *AIAA J.* **8**, 539 (1970); E. J. Valente and L. S. Bartell, *J. Chem. Phys.* **79**, 2683 (1983).

¹⁹D. P. Gory and C. F. Stevens, in *Single-Channel Recording*, edited by B. Sakmann and E. Neher (Plenum, New York, 1983), p. 53.

²⁰The tubes were provided by the Goodfellow Corporation, 800 Lancaster Avenue, Berwyn, PA 19312-1780 (Part No. FE227150/4, stainless steel No. 1.4301, Fe/Cr18/Ni10).

²¹We used the two component epoxy glue UHU Plus Endfest 300.

²²The high pressure fittings were provided by the Nova Werke AG; see Ref. 15 (straight nipples, stainless steel AISI 316 Ti, o.d.=6.35 mm, i.d.=1.6 mm, maximum pressure 7000 bar, Cat. No. 510.1435-3).

²³The 0.5 μm filters were provided by the Nova Werke AG; see Ref. 15, (tubing o.d. 6.35 mm, pressure rating 4000 bar, orifice diameter 3 mm, Cat. No. 520.5332).

²⁴E. Neher and B. Sakmann, *Nature (London)* **260**, 779 (1976).

²⁵K. T. Brown and D. G. Flaming, *Neurosci. (Oxford)* **2**, 813 (1977).

²⁶A. Cavalié, R. Grantyn, and H. D. Lux, in *Practical Electrophysiological Methods*, edited by H. Kettenmann and R. Grantyn (Wiley-Liss, New York, 1992), pp. 235-240.

²⁷B. Sakmann and E. Neher, in Ref. 19, p. 637.

- ²⁸The glass was provided by Fa. Hilgenberg GmbH, PF 1161, D-34321 Malsfeld, Germany, Cat. No 1 158 200.
- ²⁹Zeitz-Instrumente Vertriebs GmbH, Verdistrasse 2, D-86199 Augsburg, Germany; Rhema Labortechnik, Am Stegskreuz 2, D-65719 Hofheim am Taunus, Germany; Sutter Instrument Co., 40 Leveroni Ct., Novato, CA 94949.
- ³⁰Larger skimmer diameters up to 300 μm were obtained by melting a glass drop onto the tip of a small diameter skimmer and then repeating the pulling procedure.
- ³¹G. A. Bird, *Phys. Fluids* **19**, 1486 (1976).
- ³²L. Rusin (private communication).
- ³³J. Fernandez de la Mora and J. Rosell-Llompart, *J. Chem. Phys.* **91**, 2603 (1989).
- ³⁴D. Bassi, A. Boschetti, S. Marchetti, G. Scoles, and M. Zen, *J. Chem. Phys.* **74**, 2221 (1981).
- ³⁵W. Schöllkopf and J. P. Toennies, *J. Chem. Phys.* **104**, 1155 (1996).
- ³⁶J. Schmiedmayer, M. S. Chapman, C. R. Ekstrom, T. D. Hammond, St. Wehinger, and D. E. Pritchard, *Phys. Rev. Lett.* **74**, 1043 (1995).
- ³⁷W. Schöllkopf and J. P. Toennies, *Science* **266**, 1345 (1994).
- ³⁸D. M. Tenant, J. E. Bjorkholm, M. L. O'Malley, M. M. Becker, J. A. Gregus, and R. W. Epworth, *J. Vac. Sci. Technol. B* **8**, 1975 (1990); O. Carnal, M. Sigel, T. Sleator, H. Takuma, and J. Mlynek, *Phys. Rev. Lett.* **67**, 3231 (1991).
- ³⁹A helium-atom reflection scanning microscope is presently under construction in our laboratory.
- ⁴⁰W. D. Johnston and J. G. King, *Rev. Sci. Instrum.* **347**, 475 (1966).
- ⁴¹R. O. Woods and J. B. Fenn, *Rev. Sci. Instrum.* **373**, 917 (1966).
- ⁴²A. H. Shapiro, *The Dynamics and Thermodynamics of Compressible Fluid Flow* (Ronald, New York, 1953), Vol. 1, p. 159.
- ⁴³H. R. Murphy and D. R. Miller, *J. Phys. Chem.* **88**, 4474 (1984).
- ⁴⁴B. Schilling, Diplom thesis, University of Göttingen, 1989.
- ⁴⁵B. D. Esry, C. D. Liu, and Ch. Greene, *Phys. Rev. A* **54**, 394 (1996).
- ⁴⁶R. D. McCarty, *J. Phys. Chem. Ref. Data* **2**, 4 (1973).
- ⁴⁷A. R. Janzen and R. A. Aziz, *J. Chem. Phys.* **103**, 9626 (1995).